A Comparison of Geometric Imperfection Models for Collapse Analysis of Ship-Type Stiffened Plated Grillages

Shen Li[a*], Dimitris G. Georgiadis[b*], Do Kyun Kim[c,d*], Manolis S. Samuelides[b]

[a] Department of Naval Architecture, Ocean and Marine Engineering, University of Strathclyde, Glasgow, United Kingdom

[b] School of Naval Architecture and Marine Engineering, National Technical University of Athens, Greece

[c] Department of Naval Architecture and Ocean Engineering, Seoul National University, Seoul, Korea

[d] Research Institute of Marine Systems Engineering, Seoul National University, Seoul, Korea

Corresponding authors:

shen.li@strath.ac.uk (Shen Li); dgeorgiadis@central.ntua.gr (Dimitris G. Georgiadis); do.kim@snu.ac.kr (Do Kyun Kim)

Abstract: The assessment of the buckling and ultimate strength is a mandatory step in the ultimate limit state design of ship structures. The collapse analysis of ship-type stiffened panels under longitudinal compression is highly affected by initial geometric imperfection. Several geometric imperfection models are available in the literature. Broadly speaking, they can be categorised into deterministic and probabilistic approaches. The deterministic approach describes the initial deflection field with a presumed geometric shape and a characteristic maximum distortion magnitude. Several geometric deflection shapes are commonly adopted, including hungry-horse (HH) mode, Admiralty Research Establishment (ARE) mode and critical buckling (CM) mode. Each of these deflection mode shapes is used in conjunction with a characteristic maximum distortion magnitude. Except otherwise specified, an average-level magnitude is usually applied. By contrast, the probabilistic approach evaluates the initial geometric imperfection as a random field, generated based on the prescribed statistics. A

This is a peer-reviewed, accepted author manuscript of the following article: Li, S., Georgiadis, D. G., Kim, D. K., & Samuelides, M. S. (2022). A comparison of geometric imperfection models for collapse analysis of ship-type stiffened plated grillages. Engineering Structures, 250, [113480]. https://doi.org/10.1016/j.engstruct.2021.113480

comparative study is presented in this study in the light of analysing the uncertainty in ultimate compressive strength of stiffened plated grillages induced by different modelling of geometric imperfection. In addition, the influence of relative deflection in the adjacent panels is analysed. Recommendations for choosing an imperfection model for buckling analysis of ship-type stiffened plated structures are reported.

Keywords: Geometric imperfection, Buckling, Ultimate strength, Stiffened panel, Random filed.

Nomenclature

a	Plate length
b	Plate width
t	Plate thickness
σ_Y	Material yield stress of plate
E	Material elastic modulus
σ_{Yeq}	Equivalent material yield stress of stiffened panel
B	Grillage width
h_w	Stiffener web's height
t_w	Stiffener web's thickness
b_f	Stiffener flange width
t_f	Stiffener flange thickness
w_{opl}	Plate distortion
w_{oc}	Column type distortion
w_{os}	Stiffener sideway distortion
w_{opl}^{max}	Maximum magnitude of plate distortion
w_{oc}^{max}	Maximum magnitude of column type distortion
w_{os}^{max}	Maximum magnitude of stiffener sideway distortion

$\beta = b/t\sqrt{\sigma_Y/E}$	Plate slenderness ratio
$\lambda = a/(\pi k)\sqrt{\sigma_{Yeq}/E}$	Column slenderness ratio
ρ_{oc}	Relative ratio of column type distortion of adjacent bays

1. Introduction

The examination of buckling resistance and ultimate capacity, also known as the Ultimate Limit State (ULS), is a central task in the design, appraisal and optimisation of a structural system **[1-8]**. A large body of studies in the maritime sector has been devoted to this research field to investigate the influence of structural slenderness, initial imperfection, boundary condition, secondary loading, cyclic loading, dynamic loading, arctic environment, cryogenic condition, elevated temperature, corrosion, fatigue crack and accidental damage **[9-13]**. Relevant studies in other disciplines such as civil engineering may also refer to **[14-18]**.

It is a standard procedure to consider the initial geometric imperfection in buckling analysis of stiffened plated structures, which is also recognised as one of the most important influencing parameters. Many studies are available in the literature to investigate the buckling capacity of stiffened plated structures with initial geometric imperfection **[19-37]**. For a ship-type stiffened plated grillage, three different types of geometric imperfections are considered, local plate distortion, column-type distortion and stiffener sideway distortion. Regarding the column-type and stiffener sideway distortions, they are usually assumed as a single-half wave mode shape with its magnitude proportional to the panel's length. As for the local plate distortion, various geometric imperfection models are available in the literature. Broadly speaking, they can be categorised into deterministic and probabilistic approaches.

The deterministic approach approximates the initial deflection field with a presumed geometric shape and characteristic maximum distortion magnitude. Several geometric deflection shapes are commonly adopted, including hungry-horse (HH) mode **[38, 39]**, Admiralty Research Establishment (ARE) **[40-42]** mode and critical buckling (CM) mode **[43]**. In deterministic modelling, each of these deflection mode shapes is used in conjunction with a characteristic maximum distortion magnitude. Three different characteristic magnitudes may be chosen, corresponding to a slight, average, and severe level, respectively. Except otherwise specified, an average-level magnitude is usually applied. The deterministic approach provides practical modelling of the initial geometric imperfection of stiffened panels. However, these representations usually correspond to an as-built condition, which may not be applicable for in-service stiffened plated structures. After several years in service, the geometric imperfection of stiffened plated structures could be substantially different from the as-built condition, possibly due to the presence of local dents and accumulation of permanent set etc. By contrast, the probabilistic approach evaluates the initial geometric imperfection as a random field. A stochastic geometric imperfection was proposed by **[44]**, in which the random deflection fields are generated based on the first/second-order statistics and a target auto-correlation form. This model is able to consider the inherent randomness of geometric imperfection and therefore applicable for both as-built and in-service stiffened plated structures.

Very recently, a benchmark study involving seventeen participants worldwide demonstrated the uncertainty in predicting the ultimate capacity, failure mode and location of a stiffened plated grillage **[45]**. The modelling of initial distortion was suggested as one of the critical factors, which differed between each participant. Most of the existing literature on the effects of initial imperfection have only focused on the

imperfection magnitude or performed case studies on simple column structures. No research is available on the comparison of different geometric imperfection models (profile and magnitude) applied to a multi-frame and multi-bay orthogonally stiffened plated grillage.

It should be noted that the imperfection models aforementioned are all of an empirical nature. However, their developments have been based on a fairly large fairly large database, which covered the most typical manufacturing practice in the shipbuilding industry. In the light of this, they can be viewed as a generalised formula that can be applied to all ship-type stiffened panel, provided that the structures are manufactured in accordance with a standard approach. All of these formulae are well accepted by the marine structure community and widely applied in many different studies. However, there is no comparative study on these models.

In light of this, the object of this paper is to present a comparative study for different imperfection models and to provide some recommedatino on choosing an appropriate imperfection model for buckling analysis of ship-type stiffened plated structures. Collapse analyses of several ship-type stiffened plated grillages with different slenderness are completed. In addition to the comparison between different geometric imperfection models, the influence of the relative defection in the adjacent panels is also analysed. The induced uncertainty in ultimate strength will be discussed.

The remaining part of this paper will be structured as follows. A concise summary of the modelling of geometric imperfection is given in section 2 for both deterministic and probabilistic approaches. The test matrix of the comparative study is detailed in section 3. The finite element modelling for the collapse analysis of stiffened panels is given in

section 4. The insights developed from the analyses are discussed in section 5. Finally, the conclusions drawn from this comparative study are summarised in section 6.

2. Modelling of Geometric Imperfection

2.1 Principle

The initial geometric imperfection of a stiffened plated grillage is formed of three components, namely local plate distortion (w_{opl}), column-type distortion (w_{oc}) and stiffener sideway distortion (w_{os}), as shown in Figures (1) and (2).

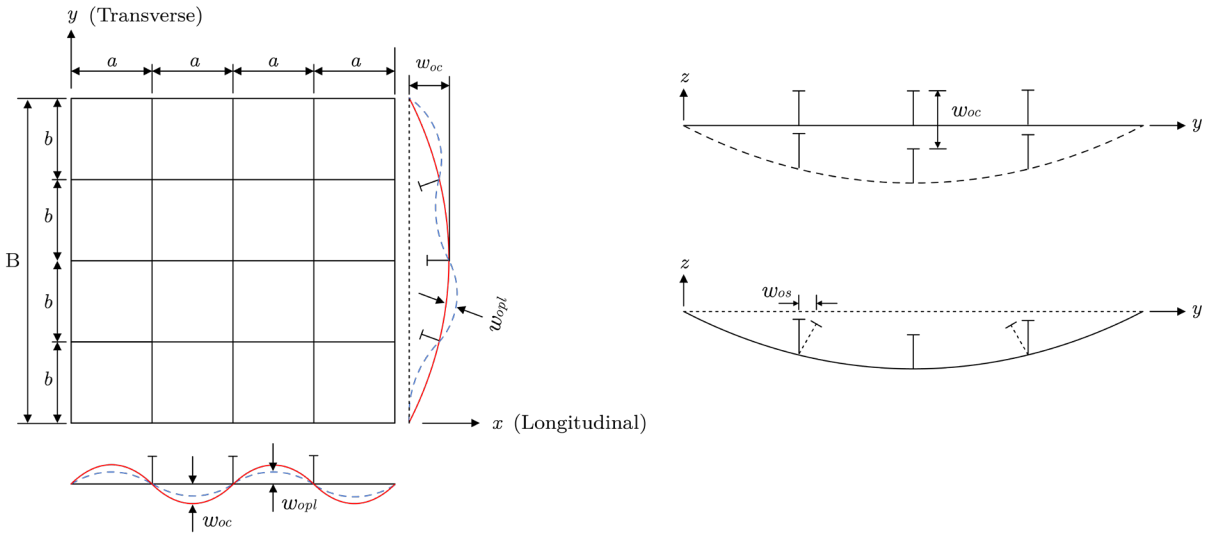

Figure 1. Schematic illustration of the initial geometric imperfection.

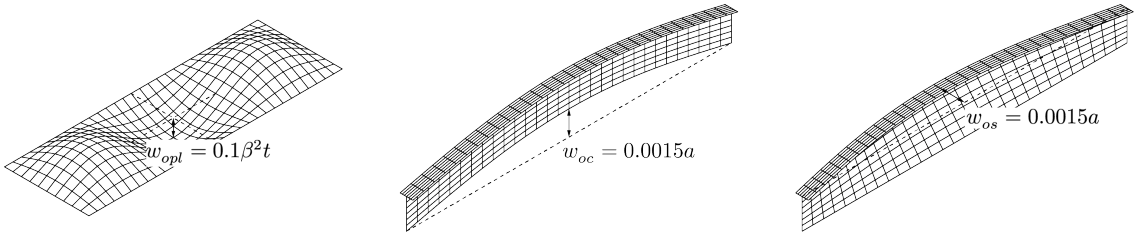

Figure 2. Examples of different types of initial deflections applied in the finite element model.

Both deterministic and probabilistic approaches are available to model the local plate distortion, whereas only a deterministic approach has been developed for modelling the column-type and stiffener sideway distortions. In the following, the prevailing geometric imperfection models are introduced.

2.2 Local Plate Distortion (Deterministic Approach)

The distortion profile and its maximum magnitude should be defined in a deterministic approach for modelling the local plate distortion. A general expression of this approach can be written as:

$$w_{opl} = w_{opl}^{max} f_{opl}(x, y) \tag{1}$$

where w_{opl}^{max} is the maximum distortion magnitude and $f_{opl}(x, y)$ is the distortion profile as a function of the spatial coordinates.

2.2.1 Distortion Profile

Three geometric imperfection profiles are commonly adopted, namely the hungry-horse (HH) mode, Admiralty Research Establishment (ARE) mode and critical buckling (CM) mode. The hungry horse mode, which is sometimes named the thin-horse mode, was proposed by **[38]** based on full-scale measurement data of ship structures. It was assumed that the deflection of the plating could be approximated by a Fourier series with eleven components, as given by Equation (2):

$$f_{opl}^{HH}(x, y) = \sum_{i=1}^{11} A_i \, sin\left(\frac{i\pi x}{a}\right) sin\left(\frac{\pi y}{b}\right) \tag{2}$$

With the aid of full-scale measurement data, a least-square regression was applied to estimate the coefficient of each Fourier component, which is summarised in Table (1). A

recent full-scale measurement by Yi et al. **[46]** may confirm the validity of a hungry-horse mode shape induced by the common welding technique in modern shipyards. In fact, an equivalent model was also developed in the field of civil engineering in earlier work **[47]**.

Table 1. Deflection coefficients of hungry-horse mode geometric imperfection model

Aspect ratio	A_1	A_2	A_3	A_4	A_5	A_6
$1 < a/b\sqrt{2}$	1.1158	-0.0276	0.1377	0.0025	-0.0123	-0.0009
$\sqrt{2} < a/b\sqrt{6}$	1.1421	-0.0457	0.2284	0.0065	0.0326	-0.0022
$\sqrt{6} < a/b\sqrt{12}$	1.1458	-0.0616	0.3079	0.0229	0.1146	-0.0065
$\sqrt{12} < a/b\sqrt{20}$	1.1439	-0.0677	0.3385	0.0316	0.1579	-0.0149
$\sqrt{20} < a/b\sqrt{30}$	1.1271	-0.0697	0.3483	0.0375	0.1787	-0.0199
Aspect ratio	A_7	A_8	A_9	A_{10}	A_{11}	
$1 < a/b\sqrt{2}$	-0.0043	0.0008	0.0039	-0.0002	-0.0011	
$\sqrt{2} < a/b\sqrt{6}$	-0.0109	0.0010	-0.0049	-0.0005	0.0027	
$\sqrt{6} < a/b\sqrt{12}$	0.0327	0.0000	0.0000	-0.0015	-0.0074	
$\sqrt{12} < a/b\sqrt{20}$	0.0743	0.0059	0.0293	-0.0012	0.0062	
$\sqrt{20} < a/b\sqrt{30}$	0.0995	0.0107	0.0537	-0.0051	0.0256	

The ARE mode is a semi-empirical imperfection representing a "real" plate whilst ensuring that the plate buckling will nucleate into an appropriate pattern **[40-42]**. As given by Equation (3), three imperfection modes are superimposed to define the complete profile, in which the first two modes (i.e. A_1 and A_j) represent a combination of realistic distortion and critical buckling, while the high-order mode (A_{j+1}) ensures that the nucleation of out-of-plane deflection occurs at one part of the plate.

$$f_{opl}^{ARE}(x,y) = \left[A_1 sin\left(\frac{\pi x}{a}\right) + A_j sin\left(\frac{j\pi x}{a}\right) + A_{j+1} sin\left(\frac{(j+1)\pi x}{a}\right)\right] sin\left(\frac{\pi y}{b}\right) \quad (3)$$

The ratio between A_1 and A_j as specified by Equation (4) is introduced based on measurements. It is unclear if any thorough regression analysis was performed, but the

proposed ratio is generally in agreement with the data reported in **[48]**. Typical values of A_1 and A_j are given in Table (2) for different aspect ratios.

$$A_1/A_j = 4.0 \tag{4}$$

In the ARE model, the half-wave number of the preferred buckling mode shape is given as:

$$j = a/b + 1, j \in \mathbb{Z} \tag{5}$$

Table 2. Deflection coefficients of ARE mode geometric imperfection model

	$j=3$	$j=4$	$j=5$	$j=6$	$j=7$	$j=8$
A_1	1.1177	0.8410	0.7998	0.8195	0.8619	0.8122
A_j	0.2794	0.2102	0.2000	0.2049	0.2155	0.2031
A_{j+1}	0.0100	0.0100	0.0100	0.0100	0.0100	0.0100

The CM mode is only constituted by one sinusoidal function, which is the preferred buckling mode of the tested plating as given by Equation (6).

$$f_{opl}^{CM}(x,y) = sin\left(\frac{m\pi x}{a}\right) sin\left(\frac{\pi y}{b}\right) \tag{6}$$

It should be noted that the half-wave number in the preferred buckling mode of the CM model is different from that in the ARE model. For the CM model, it can be determined by:

$$a/b \leq \sqrt{m(m+1)}, m \in \mathbb{Z} \tag{7}$$

In numerical simulation based on CM mode, the distortion of the plating would generally follow the initial shape up to and probably beyond the ultimate collapse. The CM mode may result in an overly conservative estimation of the ultimate strength of plates and

stiffened panels. Moreover, a significant distortion could occur from the beginning of the compressive load application, which causes an underestimation of the in-plane stiffness of the panels as compared with the other two mode shapes. However, the CM mode could help to avoid the convergence issue of numerical analysis, which is particularly useful for analysing large-scale structures. A comparison of HH, ARE and CM models is illustrated in Figure (3) for plating with aspect ratios from $a/b = 2$ to $a/b = 5$. Although the three deterministic models all belong to the Fourier series expansion method, their differences in the Fourier series terms could lead to substantial variation in predicting buckling and ultimate strength of ship-type stiffened plated structures. In addition, while the accuracy of characterisation of an actual geometric imperfections will increase with more Fourier series terms, the development of the HH model was based on a particular dataset. Its application to all ship structures and analyses still raises an uncertainty that needs to be evaluated.

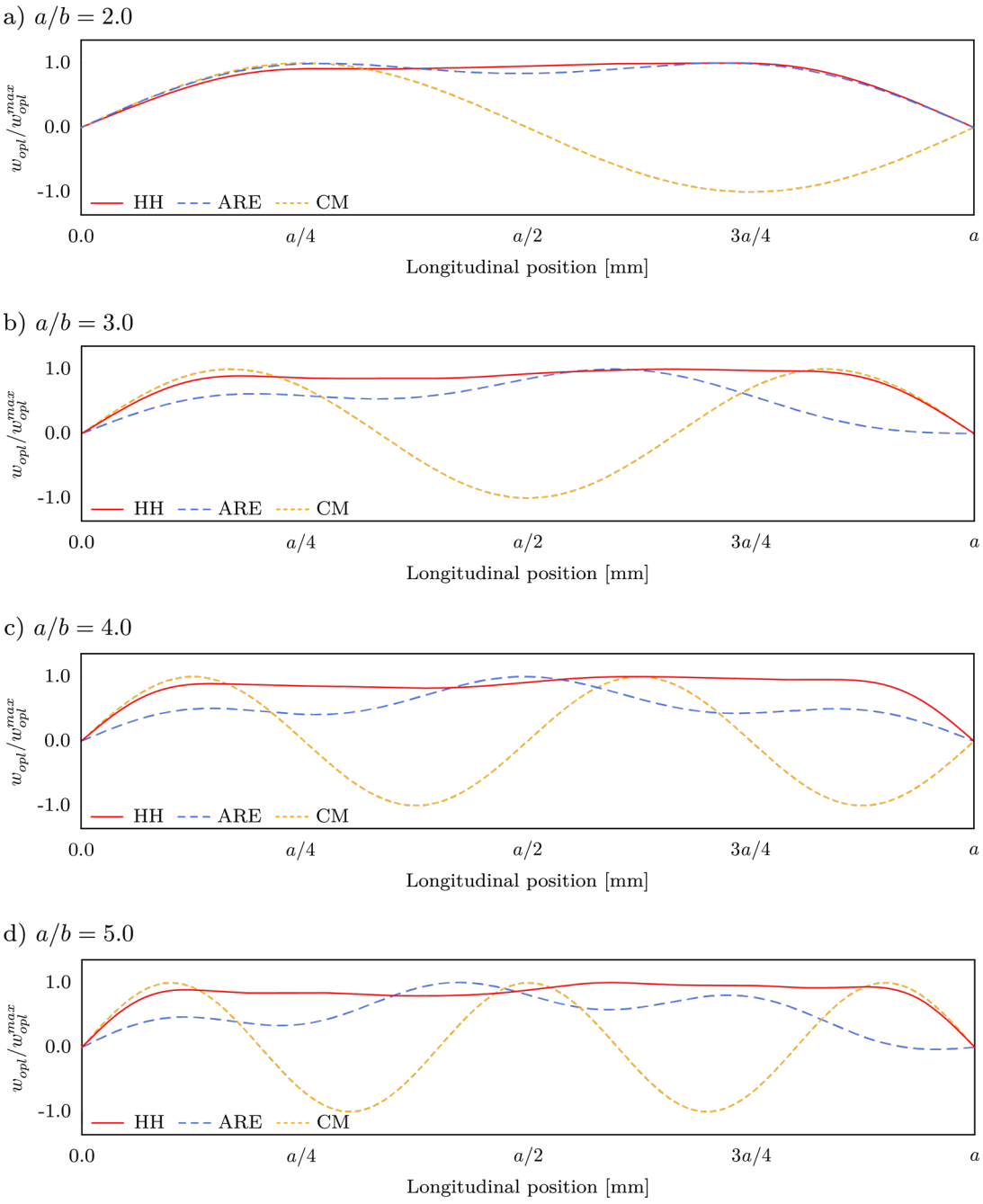

Figure 3. Comparison of HH, ARE and CM distortion profiles

2.2.2 Distortion Magnitude

Once the deterministic shape of the geometric distortion is defined, the maximum amplitude of the distortion field should be specified. The recommendation by Smith et al. **[40, 41]** is given by Equation (8) to (10), which includes three different levels of

severities given in terms of plate slenderness ratio (β) and plate thickness (t), and is developed from the measurements on full-scale ship structures.

$$w_{opl}^{max} = 0.025\beta^2 t \text{ for slight level} \quad (8)$$

$$w_{opl}^{max} = 0.1\beta^2 t \text{ for average level} \quad (9)$$

$$w_{opl}^{max} = 0.3\beta^2 t \text{ for severe level} \quad (10)$$

The slight and severe levels correspond to 3% and 97% quantiles assuming a log-normal distribution, respectively. There are different definitions of the local plate distortion magnitude in the literature, such as **[49]**, where the distortion magnitude was expressed as a function of plate width or a combination of plate width and plate thickness. However, some of these expressions were dedicated to civil engineering structures and may not be applicable in ship structures due to the difference in manufacturing practice and standards. On the contrary, Equation (8) to (10) were developed based on the measurement of ship structures and therefore appeared to be the most accepted specification of geometric imperfection magnitude. A comparison of the imperfection magnitude between the empirical formulae recommended by Smith et al. **[40, 41]** and experimental measurements summarised by Paik and Thayamballi **[50]** is shown in Figure (4). It could be suggested from this comparison that the average-level magnitude is a rational specification in ultimate strength analysis, and it appears that a severe distortion magnitude could not be found in all measurements. However, it should be noted that these measurements were completed on small-scaled structures and represented a laboratory as-built condition. The scaling effect may not be fully catered by the dimensionless parameter β and therefore lead to a deviation of the distortion magnitude between small-scaled and full-scaled structures. A comparison between Smith's formulae and several full-scale measurements was reported by **[39]**, as shown in

Figure (5). Compared with a limited database, the maximum distortion magnitude is between the average and the slight level.

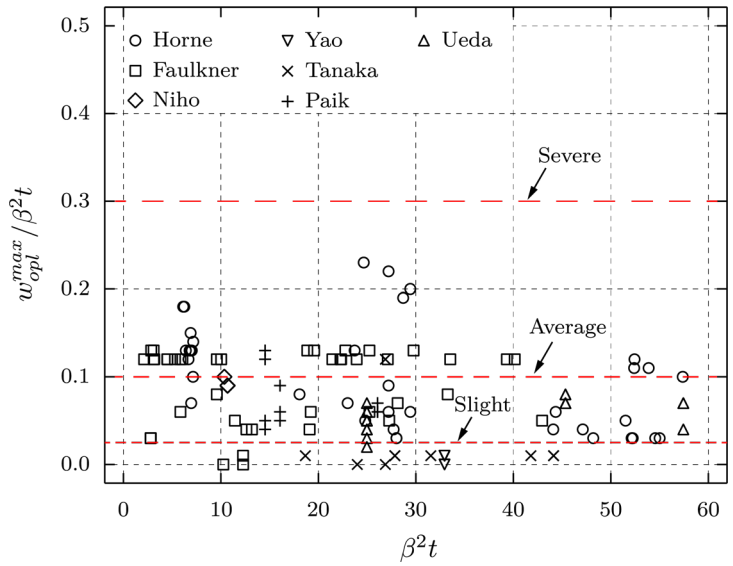

Figure 4. Comparison between Smith's formulae and small-scale measurement for the maximum local plate distortion magnitude.

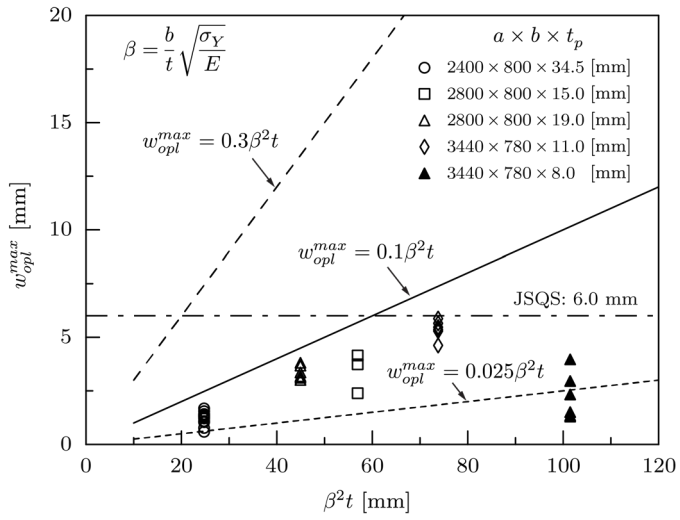

Figure 5. Comparison between Smith's formulae and full-scale measurement for the maximum local plate distortion magnitude **[39]** (Note: JSQS = Japan Shipbuilding Quality Standard).

2.3 Local Plate Distortion (Probabilistic Approach)

A stochastic geometric imperfection model was proposed by Georgiadis and Samuelides **[44]** for local plating, which is denoted as the G-S model hereafter. The schematic profile view of this stochastic model is shown in Figure (6).

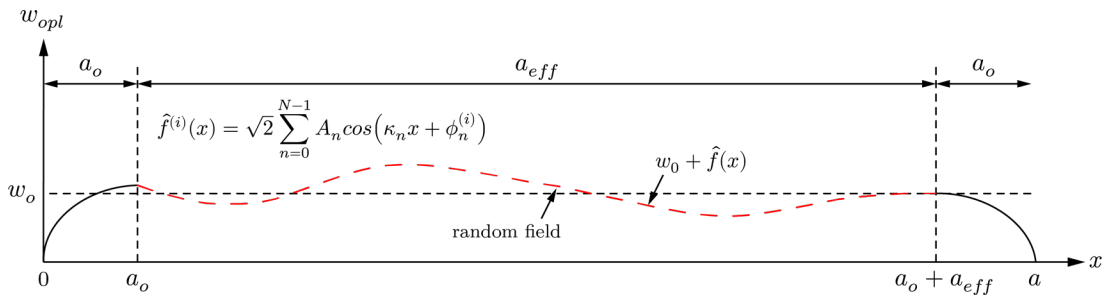

Figure 6. Schematic illustration of the stochastic geometric imperfection model.

Note that this model is a one-dimensional formulation. The stochastic geometric imperfection model aims to preserve the global dominant barrel shape while introducing random local distortion. The random field is introduced on the effective length a_{eff}. The geometric imperfection w_{eff} within the effective length is given as:

$$w_{eff}(x) = w_o + \hat{f}(x) \tag{11}$$

where w_o is the mean imperfection magnitude and $\hat{f}(x)$ is a zero-mean Gaussian stochastic field. Considering a single half-wave sinusoidal over the breadth of the plate, the full description of the local plate imperfection is given as follows:

$$w_{opl}(x,y) = w_{eff}(x = a_o)\left|sin\left(\frac{\pi x}{2a_o}\right)\right| sin\left(\frac{\pi y}{b}\right), x \in [0, a_o) \tag{12}$$

$$w_{opl}(x,y) = w_{eff}(x) sin\left(\frac{\pi y}{b}\right), x \in [a_o, a_o + a_{eff}] \tag{13}$$

$$w_{opl}(x,y) = w_{eff}\left(x = a_o + a_{eff}\right)\left|sin\left[\frac{\pi(x-a_{eff})}{2a_o}\right]\right| sin\left(\frac{\pi y}{b}\right), x \in (a_o + a_{eff}, a] \quad (14)$$

For determining the effective length a_{eff}, the following relationship could be used, which was introduced by Dow and Smith **[51]** and is universally applicable for aspect ratio.

$$a_{eff} = 0.80a \quad (15)$$

Alternatively, based on full-scale measurement, Ueda and Yao **[38]** provides an aspect ratio-dependent relations as follows:

$$a_{eff} = 0.50a, a/b \in [\sqrt{2}, \sqrt{6}) \quad (16)$$

$$a_{eff} = 0.67a, a/b \in [\sqrt{6}, \sqrt{12}] \quad (17)$$

$$a_{eff} = 0.75a, a/b \in (\sqrt{12}, \sqrt{20}] \quad (18)$$

The zero-mean Gaussian stochastic field $\hat{f}(x)$ can be realised by a series representation as follows **[52]**:

$$\hat{f}(x) = \sqrt{2}\sum_{n=0}^{N-1} A_n \, cos\left(\kappa_n x + \phi_n^{(i)}\right) \quad (19)$$

where the deterministic amplitude A_n is given by a prescribed power spectral density function S_{ff}:

$$A_n = \sqrt{2S_{ff}(\kappa_n)\Delta\kappa} \quad (20)$$

and the random phase angle $\phi_n^{(i)}$ is uniformly distributed from 0 to 2π using a Latin Hypercube Sampling (LHS) method.

$$\phi_n^{(i)} \sim U(0,2\pi) \tag{21}$$

The wave number κ_n in Equation (20) is taken as

$$\kappa_n = n\Delta\kappa \tag{22}$$

where $\Delta\kappa$ is a function of the total number of the trigonometric functions N and the cut-off wave number κ_u:

$$\Delta\kappa = \kappa_u / N \tag{23}$$

The cut-off wave number κ_u can be specified by the following criterion with $\epsilon \ll 1$, e.g. $\epsilon = 0.05$.

$$\int_0^{\kappa_u} S_{ff}(\kappa)\, d\kappa = (1-\epsilon) \int_0^{\infty} S_{ff}(\kappa)\, d\kappa \tag{24}$$

It should be noted that when generating the sample function of the simulated stochastic field, the space increment Δx has to satisfy the following condition:

$$\Delta x = \pi / \kappa_u \tag{25}$$

The power spectral density function S_{ff} suggested in **[44]** was selected based on the available measurement to fit with an auto-correlation function R_{ff} given as follows:

$$R_{ff} = \sigma_f^2 \frac{l_c^4(l_c^2 - 3|\tau^2|)}{(l_c^2 + |\tau|^2)^3} \tag{26}$$

where $|\tau| = |x_1 - x_2|$ is the relative distance between two positions, σ_f is the standard deviation of the random field and l_c is the correlation length. Using the Fourier transformation, the power spectral density function S_{ff} is given as follows:

$$S_{ff} = \frac{1}{\pi}\int_0^\infty R_{ff}(\tau)\cos(\kappa\tau)d\tau \tag{27}$$

$$S_{ff} = \frac{\sigma_f^2}{4} l_c^3 \kappa^2 exp(-l_c|\kappa|) \tag{28}$$

where κ is the wave number.

In short, in the probabilistic modelling of geometric imperfection, the w_o, σ_f and l_c are the three main inputs.

2.4 Column-Type Distortion

The column-type distortion refers to the flexural distortion of stiffener and its attached plating and is of a single half-wave sinusoidal shape in both longitudinal and transverse direction, given as:

$$w_{oc}(x,y) = w_{oc}^{max} sin\left(\frac{\pi x}{a}\right) sin\left(\frac{\pi y}{B}\right) \tag{29}$$

where w_{oc}^{max} is the maximum column-type distortion magnitude and B is the overall breadth of the entire panel.

The profile of the column-type distortion is universally accepted, and the maximum distortion magnitude is usually given as a percentage of the panel length, given as:

$$w_{oc}^{max} = C_{oc}a \tag{30}$$

Nevertheless, there are different recommendations available in the literature regarding the coefficient C_{oc}. As summarised in Table (3), Smith et al. **[41]** suggested three levels of the maximum column-type distortion magnitude and are given as a function of column slenderness ratio λ.

Table 3. Deflection coefficients of ARE mode geometric imperfection model

	Slight	Average	Severe
$\lambda \in [0.2,0.4)$	0.00025	0.0008	0.0020
$\lambda \in [0.4,0.6)$	0.00025	0.0012	0.0038
$\lambda \in [0.6,\infty)$	0.00025	0.0015	0.0046

Alternatively, ISSC **[43]** adopted a relatively conservative magnitude,

$$w_{oc}^{max} = 0.0015a \tag{31}$$

and Yao and Fujikubo **[39]** suggest a somewhat optimistic value.

$$w_{oc}^{max} = 0.0010a \tag{32}$$

Regarding the relative distortion between adjacent bays, asymmetric column distortion is equivalent to a clamped boundary condition at the frame intersection and may be assumed to be appropriate for a panel that supports significant lateral pressure from the plate side, such as hydrostatic or deck loads. However, typical imperfection patterns of British warships measured amongst others by Faulkner **[53]** showed a tendency for an asymmetric type column imperfection pattern, but with different magnitudes of maximum imperfection in each direction. Smith et al. **[41]** proposed the following ratios

of the maximum column-type distortion magnitude between adjacent bays based on full-scale measurement.

$$\rho_{oc} = -0.25, slight\ \&\ average \tag{33}$$

$$\rho_{oc} = -1, severe \tag{34}$$

However, it seems that no suggestion was reported in **[39, 43]** concerning the relative column-type distortion pattern.

2.5 Stiffener Sideway Distortion

The stiffener sideway distortion refers to the distortion of stiffener in the horizontal direction. It may have a significant impact on the torsional buckling (tripping) of stiffeners. The deterministic approach is the only available option for modelling stiffener sideway distortion at the moment, given as:

$$w_{os}(x,z) = w_{os}^{max} f_{os}(x,z) \tag{35}$$

where w_{os}^{max} is the maximum sideway distortion magnitude and $f_{os}(x,z)$ is the sideway distortion profile. The profile of the stiffener sideway distortion is usually of a single half-wave sinusoidal and linearly varies from null at the plate-stiffener intersection to the maximum at the top flange of the stiffener, as adopted in **[39, 43]**.

$$f_{os}(x,z) = \frac{z}{h_w} sin\left(\frac{\pi x}{a}\right) \tag{36}$$

Alternatively, a higher-order component may be included in addition to the single half-wave mode shape.

$$f_{os}(x,z) = \frac{z}{h_w}\left[0.8sin\left(\frac{\pi x}{a}\right) + 0.2sin\left(\frac{i\pi x}{a}\right)\right] \quad (37)$$

where $i = a/h_w$, $i \in \mathbb{Z}$.

When it comes to the maximum stiffener sideway distortion magnitude, the ISSC benchmark study **[43]** adopted:

$$w_{os}^{max} = 0.0015a \quad (38)$$

Yao and Fujikubo **[39]** suggest

$$w_{os}^{max} = 0.0010a \quad (39)$$

Regarding the relative sideway distortion between adjacent bays, it seems that no recommendation has been proposed.

3. Test Matrix

3.1 Model Characteristics

Four multi-span/multi-bay orthogonally stiffened panels, initially tested by Smith **[54]**, are adopted for the comparative study (Figure 7). The principal particulars of the four case study grillages are summarised in Table (4). The dimensionless parameters of each grillage are summarised in Table (5). Note that an elastic perfectly plastic material behaviour is assumed.

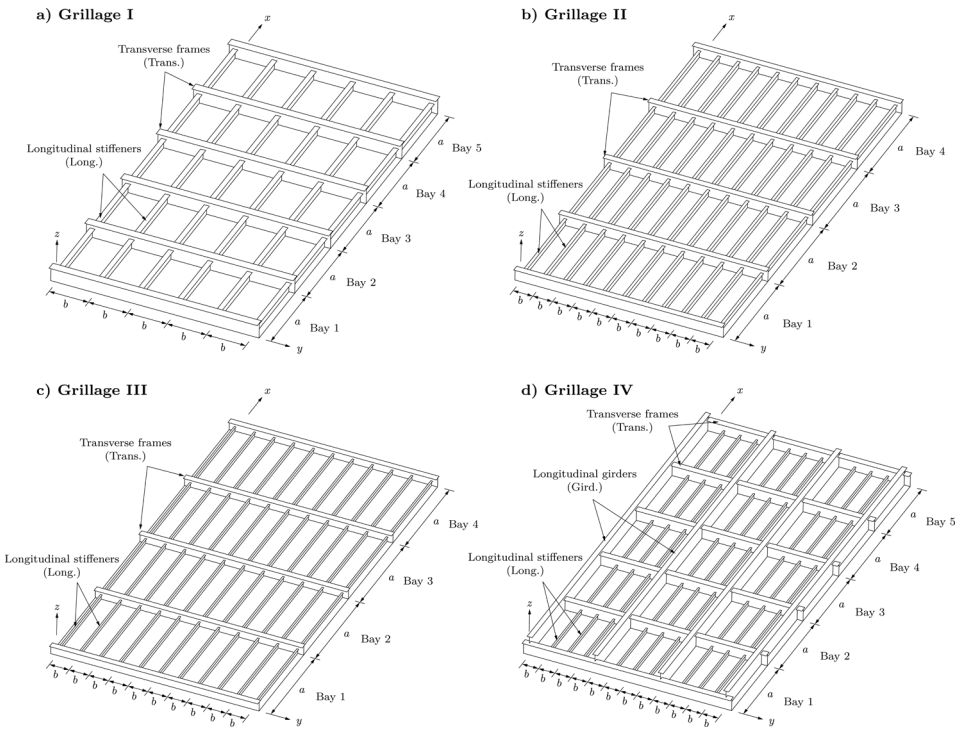

Figure 7. Case study stiffened plated grillages

Table 4. Principal particular of the case study stiffened plated grillages

Particular	Symbol	Unit	Grillage No. I	Grillage No. II	Grillage No. III	Grillage No. IV
Plate length	a	mm	1219.2	1524.0	1524.0	1219.2
Plate width	b	mm	609.6	304.8	304.8	254.0
Plate thickness	t_p	mm	8.0	7.7	6.4	6.4
Long. web height	h_w	mm	153.7	114.3	77.2	76.7
Long. web thickness	t_w	mm	7.2	5.4	4.6	4.5
Long. flange width	b_f	mm	79.0	44.7	27.9	27.7
Long. flange thickness	t_f	mm	14.2	9.5	6.4	6.4
Tran. web height	h'_w	mm	257.6	203.7	153.9	201.9
Tran. web thickness	t'_w	mm	9.3	8.3	6.9	8.6
Tran. flange width	b'_f	mm	125.5	102.6	79.2	102.4
Tran. flange thickness	t'_f	mm	18.3	16.3	14.2	16.3
Gird. web height	h''_w	mm	-	-	-	307.3
Gird. web thickness	t''_w	mm	-	-	-	6.4
Gird. flange width	b''_f	mm	-	-	-	78.0
Gird. flange thickness	t''_f	mm	-	-	-	9.5
Plate yield stress	σ_Y	MPa	226.2	237.2	228.9	235.8
Long. yield stress	σ_Y	MPa	230.3	244.1	202.7	212.4
Tran. yield stress	σ_Y	MPa	255.1	220.0	248.2	233.1
Gird. yield stress	σ_Y	MPa	-	-	-	235.8

Table 5. Dimensionless parameters of the case study stiffened plated grillages

Parameter	Symbol	Grillage No. I	Grillage No. II	Grillage No. III	Grillage No. IV
Plate slenderness ratio	β	2.67	1.42	1.68	1.41
Column slenderness ratio	λ	0.24	0.42	0.70	0.54
Length to radius of gyration	a/k	21.00	35.71	63.60	48.71

Grillage I represents relatively slender plating stiffened by stocky stiffeners. Consequently, the collapse of this panel is normally dominated by the plate buckling without distinct failure of stiffeners, which is one of the three classical buckling failure modes of ship structures as classified in **[54]** and the Mode-II failure, as categorised in **[1]**. Because of this collapse mechanism, the case study stiffened panel is appropriate to examine the uncertainty due to different geometric imperfection models for local plating. The buckling behaviour may be less sensitive to column-type and stiffener sideway imperfections. Grillage II is of intermediate slenderness ratios. The failure of this type of grillage is usually triggered by the interframe buckling of longitudinal stiffeners in combination with inelastic local plate buckling. Grillage III is the most slender panel among all case study models. Its failure is induced by the beam-column buckling. Grillage IV is similar to Grillage II in terms of slenderness but is also stiffened by several longitudinal girders, leading to a smaller transverse extent of the panel (i.e., B). These grillage models represent the most typical buckling failure modes found in ship structures. In fact, a thorough numerical analysis of multi-span/multi-bay orthogonally stiffened panels is relatively limited in the maritime sector. For this reason, the present numerical study is of significance on the collapse analysis of ship structures in the view of gaining improved insights on the uncertainty caused by initial imperfection.

3.2 Scope of Analysis

A series of analyses are performed on four stiffened plated grillages, with different models for local plate distortion (deterministic and probabilistic) and different relative distortion between adjacent bays (symmetric, asymmetric, random). A summary of the test matrix is given in Table (6).

Table 6. Summary of the test scneario matrix

	Grillage I	Grillage II	Grillage III	Grillage IV
f_{opl}	HH, ARE, CM, G-S	HH, ARE, CM	HH, ARE, CM	HH, ARE, CM
f_{oc}	Eq. 29	Eq. 29	Eq. 29	Eq. 29
f_{os}	Eq. 36	Eq. 36	Eq. 36	Eq. 36
w_{opl}^{max}	$[0.025\beta^2 t, 0.3\beta^2 t]$	$[0.025\beta^2 t, 0.3\beta^2 t]$	$[0.025\beta^2 t, 0.3\beta^2 t]$	$[0.025\beta^2 t, 0.3\beta^2 t]$
w_{oc}^{max}	$0.0015a$	$0.0015a$	$0.0015a$	$0.0015a$
w_{os}^{max}	$0.0015a$	$0.0015a$	$0.0015a$	$0.0015a$
w_o	$0.064\beta^2$	-	-	-
σ_f	$0.028\beta^2$	-	-	-
ρ_{opl}	1, -1, 0.8, rand [1, -1]	-1	-1	-1
ρ_{oc}	1, -1, rand [1, -1]	-1	-1	-1
ρ_{os}	1, -1, rand [1, -1]	-1	-1	-1

Both deterministic and probabilistic models are adopted for local plate distortion of grillage I, whereas only deterministic models are applied to grillages II, III and IV. Regarding the deterministic modelling of local plate distortion, three imperfection models, i.e., HH mode, ARE mode and CM mode, are utilised, with maximum distortion magnitude varying from $0.025\beta^2 t$ to $0.3\beta^2 t$ at an increment of $0.025\beta^2 t$ (i.e., 12 cases). When it comes to the stochastic modelling of local plate distortion of grillage I, the mean and standard deviation of the random distortion field are specified in accordance with the experimental measurement. The correlation length parameter is set equal to $l_c = 1700\text{mm}$. This value has been suggested in **[44]** based on measurements from actual plates. One hundred simulations are completed, which is considered sufficient to

compute the statistics of ultimate strength. In terms of column-type and stiffener sideway distortions, a deterministic modelling approach with fixed magnitude is employed for all grillages. As for the relative distortion between adjacent bays, symmetric ($\rho_{opl} = \rho_{oc} = \rho_{os} = 1$) and asymmetric ($\rho_{opl} = \rho_{oc} = \rho_{os} = -1$) conditions are considered for grillage I ($100 \times 2 + 12 \times 2 \times 3 = 272$ cases), whereas only the asymmetric condition is considered for grillage II, III and IV ($12 \times 3 \times 3 = 108$ cases). Two additional relative distortion scenarios are analysed for grillage I, i.e. $\rho_{opl} = 0.8$ and $\rho_{opl} = rand[1, -1]$. A random relative distortion scenario (rand[-1,1]) is analysed in conjunction with the stochastic local plate modelling for grillage I (100 cases). In this case, ρ_{opl}, ρ_{oc}, and ρ_{os} are randomly selected from -1 and 1. The scenario $\rho_{opl} = 0.8$ is considered in combination with HH mode shape (12 cases), which is a modelling technique suggested in [14]. In short, a total of (272 + 108 + 100 + 12) = 492 finite element simulations are completed.

4. Finite Element Modelling

Inconsistent with many previous studies, a four-node shell element with reduced integration is employed for the finite element modelling, which is suitable for buckling analysis of stiffened plated structures. In general, a characteristic mesh size of 50mm × 50mm is applied in the local plate discretisation. For grillage I, 24 and 12 elements are applied in the longitudinal and transverse directions, respectively. For grillage II and III, 30 and 6 elements are applied in the longitudinal and transverse directions, respectively. For grillage IV, 24 and 10 elements are applied in the longitudinal and transverse directions, respectively. In terms of the meshing of longitudinal stiffeners, 6 elements are utilised in both web and flange. When it comes to the transverse frame, a compatibly coarse meshing scheme with a typical mesh size of 100mm × 100mm is applied. The

geometric imperfection is applied to the finite element model using the direct nodal translation approach via an external subroutine **[55]**.

A simply supported boundary condition is assumed along all four edges, which is consistent with the experimental configuration reported in **[54]**. The vertical and transverse displacements at the loaded edge are constrained, while the transverse pull-in is allowed at the unloaded long edge. To ensure an uniform loading, the edge compression is applied through a master point coupled with all nodes in the loaded edge. Displacement-controlled loading combined with the arc-length solver is utilised in all cases.

5. Results and Discussions

5.1 Collapse Characteristics

The von-Mises stress distributions and deformation of four case study grillages at ULS are shown in Figure (8). It can be seen that the collapse of grillage I is predominately triggered by local plate buckling. While the yielding zone has also propagated to the longitudinal stiffeners, no significant distortion is observed at the ULS of grillage I. Nevertheless, a considerable sideway distortion of stiffeners is found in the post-collapse range.

Regarding the collapse of grillage II, a gross yielding is observed throughout the entire panel, accompanied by moderate buckling of the local plate. This is a reasonable collapse behaviour of stiffened plated structures with stocky plating.

A typical beam-column collapse failure is seen at the ULS of grillage III, where the stiffener and attached plating deflect as a combined unit. This failure mode also corresponds to the single-frame overall collapse suggested in **[1]**.

Beam-column type buckling is observed in grillage IV. In addition, a significant sideways deflection is found on the longitudinal girders of grillage IV. In fact, the elastoplastic buckling initiates at the longitudinal girders, which leads to a substantial loss of boundary support of the local panels. Subsequently, elastoplastic buckling is propagated to the plates and longitudinal stiffeners, resulting in the final collapse of the grillage.

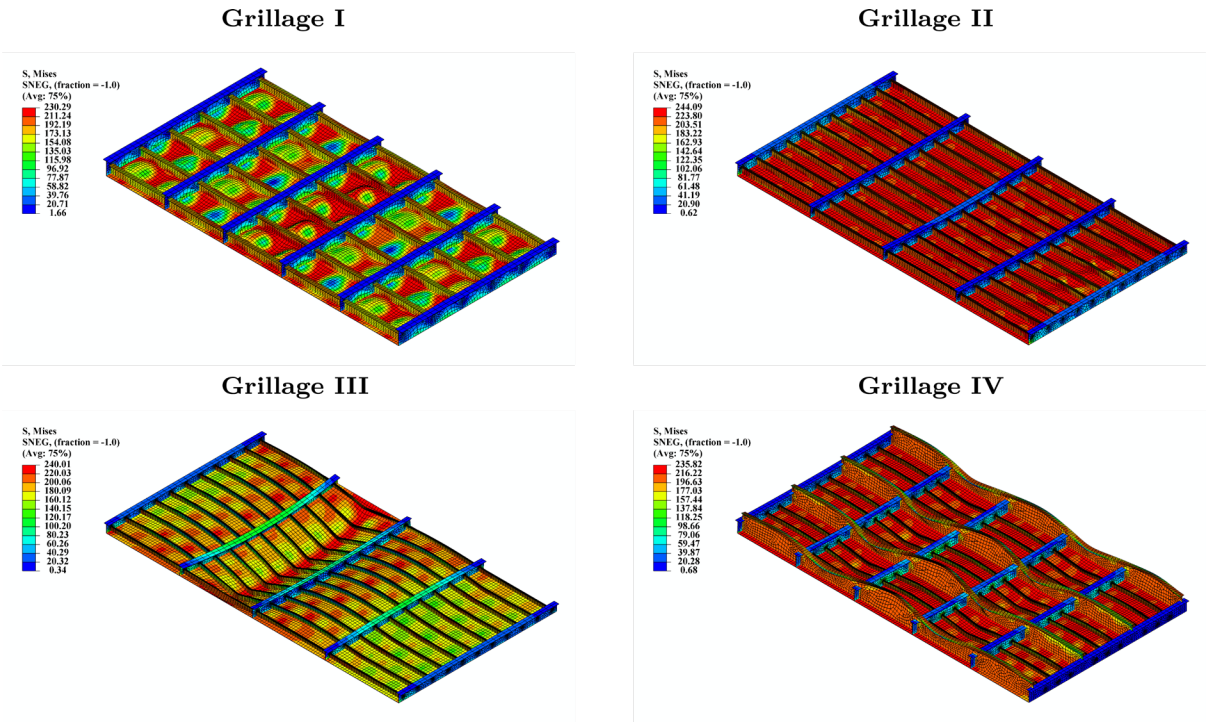

Figure 8. Stress distribution and deformation of case study grillages at ultimate limit state

5.2 Effects of Distortion Profiles

The mean ultimate compressive strength of the case study stiffened plated grillages incorporated with different deterministic imperfection models is shown in Figure (9) (Mean of 12 distortion magnitudes). Note that the presented results correspond to the asymmetric imperfection pattern, i.e. $\rho_{opl} = \rho_{oc} = \rho_{os} = -1$. It can be noted that a conservative prediction is given by the CM imperfection model. For grillages I and II, the use of the HH model gives the most optimistic prediction, while the ARE model

corresponds to an intermediate prediction. For grillages III and IV, the prediction based on HH and ARE models are close.

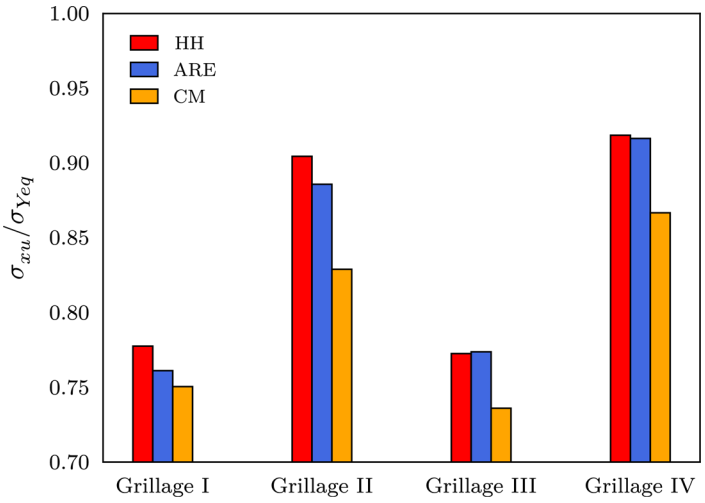

Figure 9. Mean ultimate strength of case study stiffened plated grillages (Note: mean of 12 simulations)

5.3 Effects of Distortion Magnitude

The relations between the maximum distortion magnitude (w_{opl}^{max}) and the normalised ultimate compressive strength of stiffened plated grillage (σ_{xu}/σ_{Yeq}) are shown from Figure (10) to Figure (13). Note that the presented results correspond to the asymmetric imperfection pattern, i.e. $\rho_{opl} = \rho_{oc} = \rho_{os} = -1$.

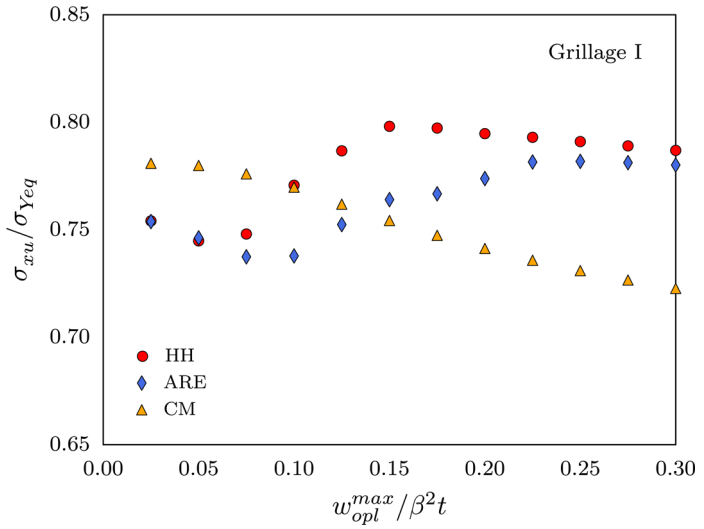

Figure 10. Relation between distortion magnitude and ultimate strength (Grillage I).

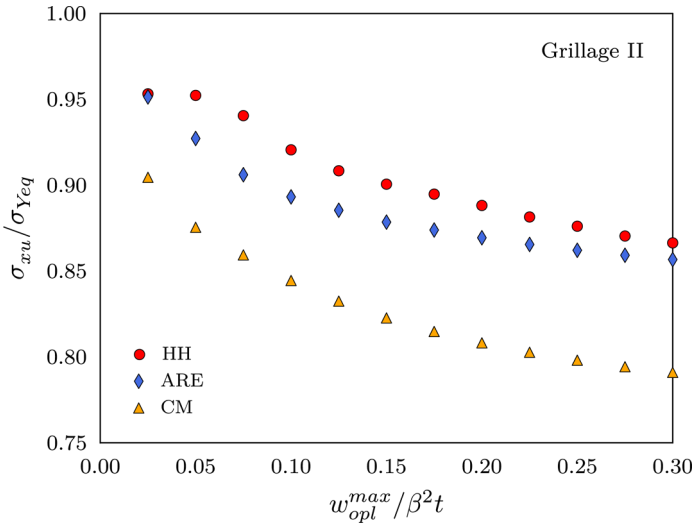

Figure 11. Relation between distortion magnitude and ultimate strength (Grillage II).

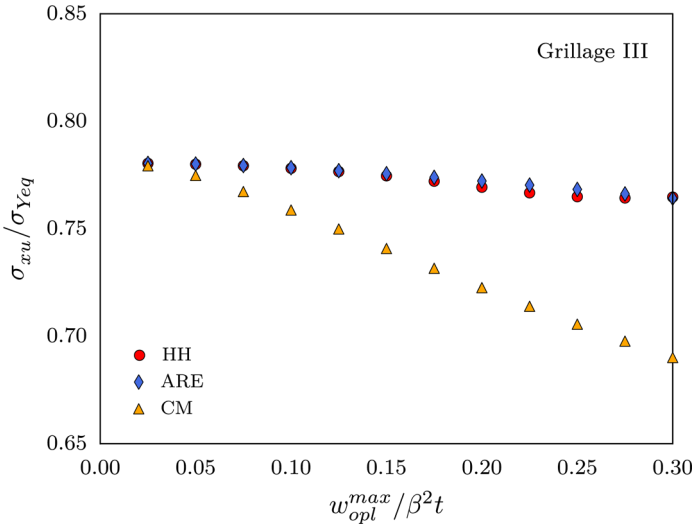

Figure 12. Relation between distortion magnitude and ultimate strength (Grillage III).

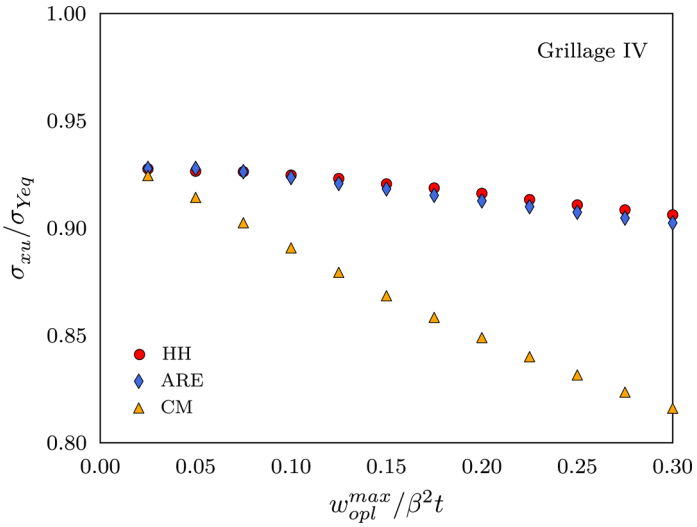

Figure 13. Relation between distortion magnitude and ultimate strength (Grillage IV).

It is evident that the ultimate compressive strength of grillage II, III and IV are reduced as the maximum local plate distortion magnitude is increased, regardless of the distortion profile. In particular, a significant reduction due to the increase of distortion magnitude is seen when the CM mode shape is assumed. Nevertheless, when HH mode and ARE mode are adopted, grillage III and grillage IV are not sensitive to the variation in distortion magnitude. This insensitivity is mainly due to the beam-column type buckling failure mode of grillages III and IV, which is not greatly governed by the local plate distortion. From these comparisons, we may arrive at the conclusion that the stiffened plated grillage is sensitive to the change of maximum magnitude of local plate distortion when the column slenderness ratio (λ) is approximately less than 0.4. For grillages with $\lambda > 0.4$, the use of CM mode shape might be conservative.

However, the foregoing monotonically decreasing relation is not observed in Figure (10) for grillage 1 when the HH or ARE mode is applied. Instead, in certain scenarios, there is an increase of the ultimate strength with a larger distortion magnitude. For instance, when the distortion magnitude is increased from $w_{opl}^{max} = 0.10\beta^2 t$ to $w_{opl}^{max} = 0.15\beta^2 t$, the ultimate compressive strength of grillage I is increased by 3.6%. This distinctive

phenomenon may be the result of interaction between the distortion components with different half-wave numbers. The deflection component other than the preferred buckling mode has a strengthening effect on the stiffened panel since it will suppress the development of out-of-plane deflection. To elucidate this, a decomposition of the deflection field of the central plating is completed for grillage I assuming ARE mode shape. The decomposition is completed using a least-square method introduced in **[39]**. In principle, the overall deflection field is approximated by eleven sinusoidal components with the half-wave number varying from 1 to 11. The coefficient of each component is estimated using a least-square method. Details of this technique are documented in the Appendix. The development of the two most significant deflection components is shown in Figure (14) for grillage 1, i.e. $i = 1$ (single half-wave) and $i = 3$ (preferred buckling shape). The vertical axis in Figure (14) represents the coefficient of the deflection component, and the horizontal axis shows the average applied strain. In the initial phase of the loading application, an increase of the deflection coefficient is shown in all cases, indicating that the local plate develops its out-of-plane deflection following the initial shape. If $w_{opl}^{max} = 0.15\beta^2 t$ (dash line), this trend keeps nearly the same until a rapid growth before the collapse. However, there is a marked turning point if $w_{opl}^{max} = 0.10\beta^2 t$ (solid line) where the deflection component with $i = 3$ keeps increasing, but the single half-wave component vanishes. The vanishing single half-wave component results in more significant development of the out-of-plane deflection in the preferred buckling mode shape, leading to a pre-mature failure of the grillage. Recalling the solid line corresponds to the lower level of distortion magnitude. This comparison may demonstrate the distinct feature of grillage I shown in Figure (10).

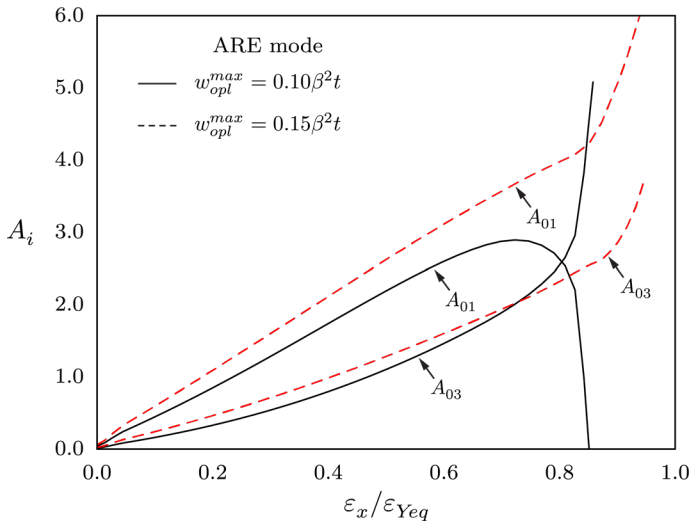

Figure 14. Development of the most significant deflection components during the progressive collapse of grillage I.

5.4 Effect of Relative Distortion in Adjacent Bays

The effects of the relative distortion in adjacent bays are illustrated in Figure (15). Generally, the relative distortion in adjacent bays has a significant influence when the HH or ARE models are adopted, leading to a prediction discrepancy of up to 12%. Conversely, the CM model shape is much less affected by the distortion in adjacent bays. In addition, it appears that the effect of relative distortion is also magnitude-dependent. It has the largest impact when the maximum distortion magnitude is about $w_{opl}^{max} = 0.05\beta^2 t$ to $w_{opl}^{max} = 0.10\beta^2 t$. However, when $w_{opl}^{max} > 0.15\beta^2 t$, the strength prediction difference based on different configurations of relative distortion is generally small.

A comparison is also illustrated for the HH model with $\rho_{opl} = 1$ and $\rho_{opl} = 0.8$. The latter configuration is recommended in **[56]**. For this case study grillage, it seems that the former case generally gives a higher prediction. However, a few exceptions are found, in which case the assumption of $\rho_{opl} = 0.8$ gives a considerably lower prediction.

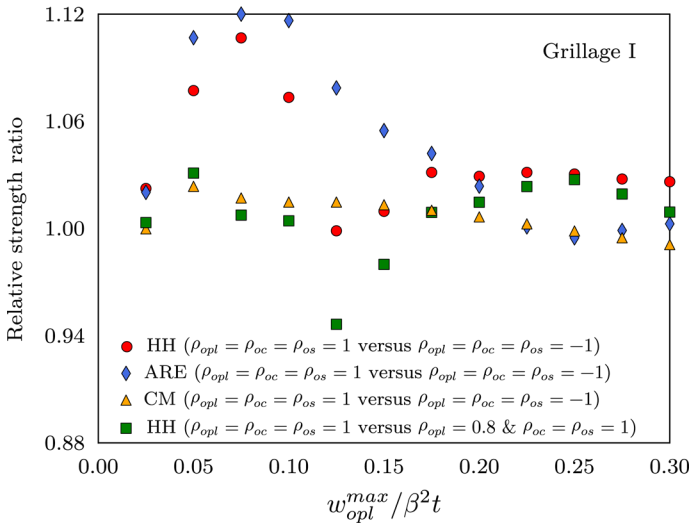

Figure 15. Effect of the relative distortion in adjacent bays on the ultimate strength of grillage

5.5 Deterministic Approach versus Probabilistic Approach

The foregoing sections have reported the results based on deterministic imperfection models. This section summarises the comparison between the deterministic approach and the probabilistic approach. A bar chart is given in Figure (16), showing the mean prediction of the ultimate strength of grillage 1 and its standard deviation.

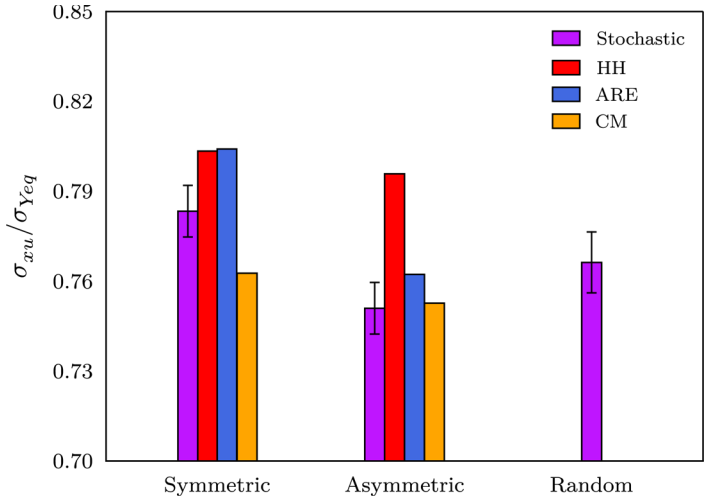

Figure 16. Comparison of ultimate strength based on deterministic and stochastic imperfection models ($w_{opl}^{max} = 0.15\beta^2 t$ for all deterministic models)

Three scenarios are considered, namely symmetric relative distortion ($\rho_{opl} = \rho_{oc} = \rho_{os} = 1$), asymmetric relative distortion ($\rho_{opl} = \rho_{oc} = \rho_{os} = -1$) and random relative distortion ($\rho_{opl} = \rho_{oc} = \rho_{os} = rand[1, -1]$). In line with the observations in the previous section, the assumption of the symmetric distortion pattern gives a higher strength prediction. A similar standard deviation is found between the predictions based on symmetric distortion pattern and asymmetric distortion pattern, while assuming a random relative distortion leads to higher prediction variance. This is probably not a surprising result since extra randomness is introduced. The computations based on deterministic models with $w_{opl}^{max} = 0.15\beta^2 t$ are also plotted in Figure (16) for comparison. Recalling that the mean and standard deviation of the local plate distortion used in the stochastic modelling of geometric imperfection are $w_{opl}^{max} = 0.064\beta^2 t$ and $w_{opl}^{max} = 0.028\beta^2 t$ respectively. Hence, a Gaussian distribution gives a maximum distortion magnitude ($w_o + 3\sigma_f$) statistically close to $w_{opl}^{max} = 0.15\beta^2 t$. It can be seen that the stochastic imperfection-based predictions are slightly conservative comparing with the HH and ARE modes, while close to the asymmetric CM mode and being optimistic with respect to the symmetric CM mode. Considering its ability to evaluate the prediction uncertainty, the G-S stochastic model is a capable alternative for modelling the geometric imperfection of stiffened plated structures.

5.6 Discussions

An appreciable discrepancy of the ultimate compressive strength resulted by different geometric imperfection models is found in all four case study grillages. It is difficult to conclusively suggest which model is the best choice for the buckling and collapse analysis

of stiffened plated structures. However, the following insights may be useful for making such a decision.

The HH model is usually the best approximation of the actual distortion field, as it is developed from full-scale measurement. However, it should be aware that it likely causes convergence issue in a nonlinear finite element simulation. This is usually due to the distortion localisation, which takes place near the ultimate limit state. It is quite often observed that the distortion near two loaded edges of the plate will significantly develop in the initial phase of loading. But when the ultimate collapse is about to occur, a rapid distortion localisation would take place in one of the loaded edges, which is usually accompanied by a snap-back response that likely leads to a convergence issue. For a stiffened panel, this convergence may be easy to resolve in most commercial finite elemnt package by tuning the incrementation step size. However, in the research of ship structures, the analysis of the structural capacity of an entire ship or cross section (single or multiple) are often needed. The degrees of freedom involved in these analyses will be extremely large and therefore it might be difficult to resolve the convergence issue.

The ARE model is generally close to the HH model in terms of the ultimate strength prediction. It is also less affected by the convergence issue aforementioned. Nonetheless, future research may be required to justify the ratio between the coefficients of a single half-wave component A_1 and critical buckling component A_j, which is now tentatively assumed as $A_1/A_j = 4.0$.

If one would like to greatly eliminate the aforementioned convergence issue due to distortion localisation, the use of the CM model is recommended. This will become particularly useful when the buckling behaviour of a large-scale structure (e.g. ship hulls) is analysed. However, it should be noted that the CM model is perhaps the worst

imperfection shape, and the prediction based on this model is generally more conservative, especially the post-collapse response.

In terms of the relative distortion pattern, both symmetric and asymmetric patterns can be adopted. This choice is mainly related again to the convergence issue and therefore also depends on the purpose of finite element simulation.

Indisputably, the inherent randomness of imperfect geometry motivates the use of a probabilistic imperfection model. The applied G-S stochastic imperfection model aims at capturing the real distortion field by retaining the global barrel shape of a plate, as a result of manufacturing processes, while accommodating the random localized dents lengthwise, mainly, as a result of impact loads during operation. To this end, the G-S model can potentially provide a more sophisticated description of the real distortion field. It is, however, acknowledged that the use of the G-S model is more complicated in practice. Further data should be acquired, in both as-built and service conditions, further data should be acquired to tune the statistics (i.e. mean deflection and standard deviation) and the auto-correlation form of the model.

6. Concluding Remarks

Geometric imperfection is one of the most crucial parameters of influence in the buckling analysis of stiffened plated structures. Several geometric imperfections are available, including deterministic and probabilistic approaches. A comparison of the prevailing geometric imperfection models and their influence on the ultimate compressive strength of ship grillages is completed in this paper. The following insights are developed from this study.

Different geometric imperfection models lead to an appreciable uncertainty in the ultimate compressive strength of ship-type stiffened plated grillages. The uncertainty is caused by the assumed distortion mode and the relative distortion pattern. These differences also have an implication in the convergence of numerical simulation. The purpose of simulation should be taken into account when choosing the geometric imperfection model, i.e. whether a more realistic structural response is desired or a robust prediction is aimed for. The use of stochastic modelling improves the deterministic approach by considering a wide spectrum of imperfect profiles whose geometry resembles real-life.

Based upon the insights developed in this study, future research could be directed to 1) measurement of the distortion of ship structures in both as-built and in-service conditions, in particular for the stiffener distortions; 2) improvement of the stochastic geometric imperfection model; 3) extended the analysis to investigate the effects of column-type imperfection and stiffener sideway imperfection; 4) development of alternative random imperfection model based on Karhunen–Loève expansion and Fourier series expansion.

References

[1] J. K. Paik, Ultimate limit state design of steel-plated structures, John Wiley Sons, Inc., 2018.

[2] Z. Xiong, S. J. Zhu, X. Z. Zou, S. Y. Guo, Y. Qiu, L. J. Li, Elastoplastic buckling behaviour of aluminium alloy single-layer cylindrical reticulated shells with gusset joints, Engineering Structures 242 (2021) 112562.

[3] Z. Y. Sun, Z. K. Lei, R. X. Bai, H. Jiang, J. C. Zou, Y. Ma, C. Yan, Prediction of compression buckling load and buckling mode of hat stiffened panels using artificial neural network, Engineering Structures 242 (2021) 112275.

[4] S. M. Zhou, J. Z. Tong, G. S. Tong, Global buckling design of multicelled cfst walls with four simply-supported edges, Thin-Walled Structures 165 (2021) 107966.

[5] Y. Hilali, O. Bourihane, A mixed mls and hermite-type mls method for buckling and postbuckling analysis of thin plates, Structures 33 (2021) 2349–2360.

[6] A. R. Nazari, F. Taheri, A parametric study into the influence of strain hardening slope on the stability and collapse responses of steel tubes under compressive loading, Structures 33 (2021) 2152–2165.

[7] C. Mercier, A. Khelil, F. Al Mahmoud, J. L. Blin-Lacroix, A. Pamies, Experimental investigations of buckling behaviour of steel scaffolds, Structures 33 (2021) 433–450.

[8] S. Li, D. K. Kim, S. Benson, A probabilistic approach to assess the computational uncertainty of ultimate strength of hull girders, Reliability Engineering & System Safety 213 (2021) 107688.

[9] S. Benson, J. Downes, R. Dow, Load shortening characteristics of marine grade aluminium alloy plates in longitudinal compression, Thin-Walled Structures 70 (2013) 19–32.

[10] S. Benson, J. Downes, R. Dow, Compartment level progressive collapse analysis of lightweight ship structures, Marine Structures 31 (2013) 44– 62.

[11] S. Benson, J. Downes, R. Dow, Overall buckling of lightweight stiffened panels using an adapted orthotropic plate method, Engineering Structures 85 (2015) 107–117.

[12] S. Tanaka, D. Yanagihara, A. Yasuoka, M. Harada, S. Okazawa, M. Fujikubo, T. Yao, Evaluation of ultimate strength of stiffened panels under longitudinal thrust, Marine Structures 36 (2014) 21–50.

[13] K. Woloszyk, Y. Garbatov, J. Kowalski, L. Samson, Experimental and numerical investigations of ultimate strength of imperfect stiffened plates of different slenderness, Polish Maritime Research 27 (4) (2020) 120–129.

[14] Timmers, R., Schwienbacher, M., Lang, R., Lener, G., 2018. Proposal and validation of a simplified numerical buckling check for stiffened plated elements. In: Proceeding of 8th International Conference on Thin-Walled Structures, Lisbon, Portugal.

[15] Timmers, R., Neulichedl, T., 2019. Calibration of design buckling curves for lateral-torsional buckling of cantilever beams made of glass - experimental and numerical investigations. Applied Sciences, 9(16), 3432.

[16] Sofıyev, A.H., Kuruoglu, N., 2013. Large-amplitude vibration of the geometrically imperfect FGM truncated conical shell. Journal of Vibration and Control, 21(1), 142-156.

[17] Haciyev, V.C., Sofiyev, A.H., Kuruoglu, N., 2019. On the free vibration of orthotropic and inhomogeneous with spatial coordinates plates resting on the inhomogeneous viscoelastic foundation. Mechanics of Advanced Materials and Structures, 26(10), 886-897.

[18] Avey, M., Yusufoglu, E., 2020. On the solution of large-amplitude vibration of carbon nanotube-based double-curved shallow shells. Mathematical Methods in the Applied Sciences, 1-13.

[19] J. M. Gordo, Effect of initial imperfections on the strength of restrained plates, Journal of Offshore Mechanics and Arctic Engineering 137 (2015) 051401.

[20] J. K. Paik, A. Thayamballi, J. M. Lee, Effect of initial deflection shape on the ultimate strength behavior of welded steel plates under biaxial compressive loads, Journal of Ship Research 48 (2004) 45–60.

[21] Z. F. Guo, R. X. Bai, Z. K. Lei, H. Jiang, J. C. Zou, C. Yan, Experimental and numerical investigation on ultimate strength of laser-welded stiffened plates considering welding deformation and residual stresses, Ocean Engineering 234 (2021) 109239.

[22] Timmers, R., Lener, G., 2016. Collapse mechanisms and load-deflection curves of unstiffened and stiffened plated structures from bridge design. Thin-Walled Structures, 106, 448-458.

[23] Timmers, R., 2021. Influence of the imperfection shapes on the collapse mechanisms of stiffened plates with Class 4 trapezoidal stiffeners. In: Proceedings of the 8th International Conference on Coupled Instabilities in Metal Structures (CIMS 2021), Lodz University of Technology, Poland.

[24] Sofiyev, A.H., 2011. Influence of the initial imperfection on the non-linear buckling response of FGM truncated conical shells. International Journal of Mechanical Sciences, 53(9), 753-761.

[25] S. F. Estefen, J. H. Chujutalli, C. Guedes Soares, Influence of geometric imperfections on the ultimate strength of the double bottom of a suezmax tanker, Engineering Structures 127 (2016) 287–303.

[26] K. N. Anyfantis, Evaluating the influence of geometric distortions to the buckling capacity of stiffened panels, Thin-Walled Structures 140 (2019) 450–465.

[27] J. P. Martins, D. Beg, F. Sinur, L. Sim˜oes da Silva, A. Reis, Imperfection sensitivity of cylindrically curved steel panels, Thin-Walled Structures 89 (2015) 101–115.

[28] M. A. Wadee, M. Farsi, Imperfection sensitivity and geometric effects in stiffened plates susceptible to cellular buckling, Structures 3 (2015) 172–186.

[29] T. Xia, P. Yang, K. Hu, C. Cui, Combined effect of imperfections on ultimate strength of cracked plates under uniaxial compression, Ocean Engineering 150 (2018) 113–123.

[30] K. Woloszyk, P. M. Bielski, Y. Garbatov, T. Mikulski, Photogrammetry image-based approach for imperfect structure modelling and FE analysis, Ocean Engineering 223 (2021) 108665.

[31] Wagner, H.N.R., Hühne, C., Niemann, S., Tian, K., Wang, B., Hao, P., 2018. Robust knockdown factors for the design of cylindrical shells under axial compression: Analysis and modeling of stiffened and unstiffened cylinders. Thin-Walled Structures, 127, 629-645.

[32] Wagner, H.N.R., Hühne, C., 2018. Robust knockdown factors for the design of cylindrical shells under axial compression: potentials, practical application and reliability analysis. International Journal of Mechanical Sciences, 135, 410-430.

[33] Wang, B., Zhu, S.Y., Hao, P., Bi, X.J., Du, K.F., Chen, B.Q., Ma, X.T., Chao, Y.J., 2018. Buckling of quasi-perfect cylindrical shell under axial compression: A combined experimental and numerical investigation. International Journal of Solids and Structures,130-131, 232-247.

[34] Hao, P., Wang, B., Li, G., Meng, Z., Tian, K., Zeng, D.J., Tang, X.H., 2014. Worst Multiple Perturbation Load Approach of stiffened shells with and without cutouts for improved knockdown factors. Thin-Walled Structures, 82, 321-330.

[35] Hao, P., Wang, B., Tian, K., Du, K.F., Zhang, X., 2015. Influence of imperfection distributions for cylindrical stiffened shells with weld lands. Thin-Walled Structures, 93, 177-187.

[36] Wang, B., Yang, M., Zeng, D.J., Hao, P., Li, G., Liu, Y., Tian, K., 2021. Post-buckling behavior of stiffened cylindrical shell and experimental validation under non-uniform external pressure and axial compression. Thin-Walled Structures, 161, 107481.

[37] Liang, K., Hao, P., Wang, B., Sun, Q., 2020. A novel reduced-order modeling method for nonlinear buckling analysis and optimization of geometrically imperfect cylinders.

International Journal for Numerical Methods in Engineeringthis link is disabled, 122(6), 1456-1475.

[38] Y. Ueda, T. Yao, The influence of complex initial deflection modes on the behaviour and ultimate strength of rectangular plates in compression, Journal of Constructional Steel Research 5 (1985) 265–302.

[39] T. Yao, M. Fujikubo, Buckling and ultimate strength of ship and ship-like floating structures, Butterworth-Heinemann, 2016.

[40] C. Smith, P. Davidson, J. Chapman, P. Dowling, Strength and stiffness of ships' plating under in-plane compression and tension, Transaction of RINA 130 (1987) 277–293.

[41] C. Smith, P. Davidson, J. Chapman, P. Dowling, Strength of stiffened plating under combined compression and lateral pressure, Transaction of RINA 134 (1991) 131–147.

[42] S. Benson, J. Downes, R. Dow, Ultimate strength characteristics of aluminium plates for high-speed vessels, Ships and Offshore Structures 6 (2011) 67–80.

[43] ISSC, Ultimate strength committee, in: 18th International Ship and Offshore Structures Congress, Rostock, Germany, 2012, pp. 25–30.

[44] D. G. Georgiadis, M. S. Samuelides, Stochastic geometric imperfections of plate elements and their impact on the probabilistic ultimate strength assessment of plates and hull-girders, Marine Structures 76 (2021) 102920.

[45] J. W. Ringsberg, I. Darie, K. Nahshon, G. Shilling, M. A. Vaz, S. Benson, L. Brubak, G. Q. Feng, M. Fujikubo, M. Gaiotti, Z. Q. Hu, B. S. Jang, J. K. Paik, M. Slagstad, K. Tabri, Y. K. Wang, B. Wiegard, D. Yanagihara, The issc 2022 committee iii.1-ultimate strength benchmark study on the ultimate limit state analysis of a stiffened plate structure subjected to uniaxial compressive loads, Marine Structures 79 (2021) 103026.

[46] M. S. Yi, D. H. Lee, H. H. Lee, J. K. Paik, Direct measurements and numerical predictions of welding-induced initial deformations in a fullscale steel stiffened plate structure, Thin-Walled Structures 153 (2020) 106786.

[47] Massonnet, Ch. Tolerances in Steel Plated Structures. IABSE Surveys S-14/80, IABSE; Zürich: 1980.

[48] C. A. Carlsen, J. Czujko, The specification of post-welding distortion tolerances for stiffened plates in compression, The Structural Engineer 54A (1978) 133–141.

[49] P. J. Dowling, S. Chatterjee, P. A. Frieze, Experimental and predicted collapse behaviour of rectangular steel box girders, in: International Conference on Steel Box Girder Bridges, 1973.

[50] J. K. Paik, A. K. Thayamballi, An empirical formulation for predicting the ultimate compressive strength of stiffened panels, in: Proceedings of the 7th International Offshore and Polar Engineering Conference, 1997.

[51] R. S. Dow, R. S. Smith, Effects of localized imperfections on compressive strength of long rectangular plates, Journal of Constructional Steel Research 4 (1) (1984) 51–76.

[52] Shinozuka, M., Deodatis, G., 1991. Simulation of stochastic processes by spectral representation. Applied Mechniacs Review, 44(4), 191-204.

[53] D. Faulkner, A review of effective plating for use in the analysis of stiffened plating in bending and compression, Journal of Ship Research 19 (1975) 1–17.

[54] C. S. Smith, Compressive strength of welded steel ship grillages, Transactions of the Royal Institution of Naval Architects 117 (1975) 249–268.

[55] S. Benson, J. Downes, R. S. Dow, An automated finite element methodology for hull girder progressive collapse analysis, In: 13th International Marine Design Conference, 2012.

[56] Tanaka, S., Yanagihara, D., Yasuoka, A., Harada, M., Okazawa, S., Fujikubo, M., Yao, T., 2014. Evaluation of ultimate strength of stiffened panels under longitudinal thrust. Marine Structures, 36, 21-50.

Appendix

As reported in [81], the deflection field of local plating w_{opl} in the longitudinal direction can be approximated by a series of sinusoidal functions where N = 11 is usually sufficient:

$$w_{opl} \approx \sum_{i=1}^{N} A_i sin\left(\frac{i\pi x}{a}\right) \quad (40)$$

For node at x_n, the vertical deflection can be estimated by Equation (40) as:

$$w_{opl}(x_n) \approx \sum_{i=1}^{N} A_i sin\left(\frac{i\pi x_n}{a}\right) \quad (41)$$

The residual (= error) between the estimation and the actual value can be written as:

$$r = w_{opl}(x_n) - \sum_{i=1}^{N} A_i sin\left(\frac{i\pi x_n}{a}\right) \quad (42)$$

A least-square problem can be formulated by taking the sum of the square of each residual:

$$R = \sum_{1}^{n} \left[w_{opl}(x_n) - \sum_{i=1}^{N} A_i sin\left(\frac{i\pi x_n}{a}\right)\right]^2 \quad (43)$$

The best-fit coefficients can be estimated by enforcing the condition that the derivative of the R with respective to each coefficient equals to zero:

$$\frac{\partial R}{\partial A_i} = 0 \tag{44}$$

A system of linear equations can then be formulated:

$$\mathbf{H} \cdot \mathbf{A} = \mathbf{W} \tag{45}$$

where

$$\mathbf{A} = \{A_1 \quad A_2 \quad \cdots \quad A_i \quad \cdots \quad A_N\}^T \tag{46}$$

$$\mathbf{W} = \{W_1 \quad W_2 \quad \cdots \quad W_i \quad \cdots \quad W_N\}^T \tag{47}$$

$$\mathbf{H} = \begin{bmatrix} H_{11} & H_{12} & \cdots & H_{1j} & \cdots & H_{1N} \\ H_{21} & H_{22} & \cdots & H_{2j} & \cdots & H_{2N} \\ \vdots & \vdots & \ddots & \vdots & \cdots & \vdots \\ H_{i1} & H_{i2} & \cdots & H_{ij} & \cdots & H_{iN} \\ \vdots & \vdots & \cdots & \vdots & \ddots & \vdots \\ H_{N1} & H_{N2} & \cdots & H_{Nj} & \cdots & H_{NN} \end{bmatrix} \tag{48}$$

The entries in **H** and **W** can be written as the following two general expressions:

$$H_{ij} = \sum_{i=1}^{N} \sum_{j=1}^{N} sin\left(\frac{i\pi x}{a}\right) sin\left(\frac{j\pi x}{a}\right), i = 0,1,2,\cdots,N \;\&\; j = 0,1,2,\cdots,N \tag{49}$$

$$W_i = \sum_{1}^{n} sin\left(\frac{i\pi x_n}{a}\right) w_{opl}(x_n), i = 0,1,2,\cdots,N \tag{50}$$